1-1-2009

Atlas of tilted accretion discs and source to negative superhumps

M. M. Montgomery
University of Central Florida

Atlas of tilted accretion discs and source to negative superhumps

M. M. Montgomery⋆

Department of Physics, University of Central Florida, Orlando, FL 32816, USA

ABSTRACT

Using smoothed particle hydrodynamics, we numerically simulate steady-state accretion discs for cataclysmic variable dwarf novae systems that have a secondary-to-primary mass ratio $0.35 \leq q \leq 0.55$. After these accretion discs have come to quasi-equilibrium, we rotate each disc out of the orbital plane by $\delta = (1, 2, 3, 4, 5$ or $20)^\circ$ to induce negative superhumps. For accretion discs tilted 5°, we generate light curves and associated Fourier transforms for an atlas on negative superhumps and retrograde precession. Our simulation results suggest that accretion discs need to be tilted more than 3° for negative superhumps to be statistically significant. We also show that if the disc is tilted enough such that the gas stream strikes a disc face, then a dense cooling ring is generated near the radius of impact.

In addition to the atlas, we study these artificially tilted accretion discs to find the source to negative superhumps. Our results suggest that the source is additional light from innermost disc annuli, and this additional light waxes and wanes with the amount of gas stream overflow received as the secondary orbits. The nodes, where the gas stream transitions from flowing over to under the disc rim (and vice versa), precess in the retrograde direction.

Key words: accretion, accretion discs – hydrodynamics – methods: numerical – binaries: close – novae, cataclysmic variables.

1 INTRODUCTION

Variability in non-magnetic, cataclysmic variable (CV), dwarf novae (DN) close binaries has been largely attributed to instabilities in their accretion discs. Two distinct instabilities have been found to lead to two different outcomes – a thermal and viscous instability results in CV classical novae, recurrent novae and DN outbursts whereas a tidal instability results in CV DN SU UMa and nova-like (NL) outbursts. The former, normal outbursts, involves cycling from low-to-high thermal and viscous states (see e.g. Meyer & Meyer-Hofmeister 1981, and references within) and thus cycling from low-to-high mass transfer rates (see e.g. Lasota 2001). The latter, larger amplitude, longer duration superoutbursts show characteristic hump-shaped modulations, known as superhumps, in their light curves. Fig. 1 (Montgomery 2004) shows a CV family tree, and this work involves the DN and NL branches. All classes shown in this tree are discussed in, for example, Smith (2006), Warner (2003) and Hellier (2001).

Observed superhump modulations in light curves are either positive if their periods are a few per cent longer than the orbital period or negative if their periods are a few per cent shorter than the orbital period. Positive superhumps (see e.g. Patterson 1998; Warner 2003) are believed to result from tidal stressing of the disc by the secondary star (see e.g. Vogt 1982; Osaki 1985; Whitehurst 1988a,b;

Hirose & Osaki 1990; Lubow 1991a,b; Whitehurst & King 1991; Whitehurst 1994; Murray 1996; Foulkes et al. 2004). With the right conditions in viscosity, mass transfer rate and secondary-to-primary mass ratios, the disc can outwardly expand to near the 3:1 eccentric inner Lindblad resonance (Whitehurst 1988a; Lubow 1991a) radius where the disc becomes eccentric (e.g. Lubow 1991b; Smith et al. 2007) and is forced to change shape cyclically from circular to elliptical (see e.g. Simpson & Wood 1998; Smith et al. 2007). The disc, however, does not remain stable. Osaki (1989) attributes the larger amplitude, longer duration superoutburst to an enhanced viscous torque that acts on the disc once the disc becomes eccentric. Numerical simulations show that the disc begins to slosh back and forth around the primary (see e.g. Lubow 1991b; Simpson & Wood 1998) and the line of apsides of the oscillating disc slowly precesses in the prograde direction. The secondary meets the line of apsides with a period that is slightly longer than the orbital period P_{orb}. This slightly longer period is the positive superhump period P_+. The positive superhump modulation in the light curve is attributed to disc dissipation from the enhanced spiral density waves created within the disc (Smith et al. 2007). Both CV DN SU UMa and permanent superhump (PS) (Patterson 1999) systems show positive superhumps in their light curves. CV DN SU UMa and PS systems have low- and high-mass transfer rates, respectively, as shown in Fig. 2 (Montgomery 2004, after a figure by Osaki 1985). The upper right quadrant, labelled NLs, refers to the magnetic NLs. The upper left quadrant, labelled PSs, refers to non-magnetic NLs. Weak IPs are in between.
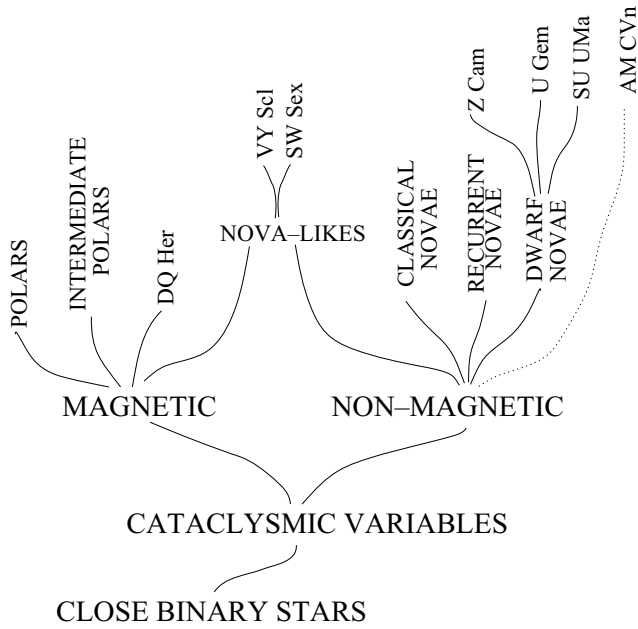
⋆E-mail: montgomery@physics.ucf.edu

Figure 1. Partial hierarchy of close binary systems from general (base) to more specific (top). Mostly hydrogen systems are shown with a solid line and mainly helium systems are shown with a dotted line.
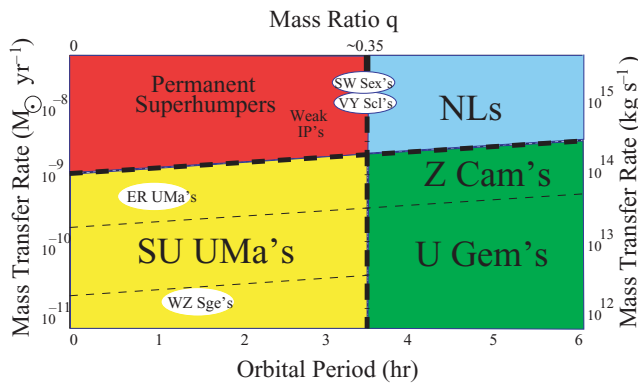

Figure 2. Various CV systems from Fig. 1 shown relative to their general orbital periods, mass ratio and mass transfer rates. Dashed lines indicate approximate locations of transition zones.

Unlike positive superhump theory, negative superhump theory is not as well established. For example, a consensus to the source of the negative superhump has not yet been achieved. Barrett, O'Donoghue & Warner (1988) suggest that the source to the negative superhump is due to the varying kinetic energy of the gas stream as it impacts one face of a disc through a locus of points as the secondary orbits the centre of mass. Patterson et al. (1997) suggest that if the disc is tilted, then the gas stream can easily flow over the top and crash down on the inner disc and thus the source to the negative superhump is gravitational energy. Wood, Montgomery & Simpson (2000) suggest that the source to the negative superhump is the tidal field disturbing the fluid flow in each of the two disc halves. Kaygorodov et al. (2006) suggest the negative superhump may be due to an inner annulus bright spot that spreads due to diffusion and that is caused by matter flowing along a one-armed

spiral density wave. Wood & Burke (2007) agree with Barrett et al. (1988) that the negative superhump modulation is from the bright spot transiting across each face of the tilted disc. Because negative superhumps are found to exist alone in CV DN systems as well in systems that show both positive and negative superhumps and because the positive superhump modulation is suggested to come from the disc (Smith et al. 2007), we suggest in this work that the source to the negative superhump must also come from the disc and from a location that is different from that which powers the positive superhump modulation.

A second unknown is whether or not the accretion disc is warped or tilted. Petterson (1977), Murray & Armitage (1998), Terquem & Papaloizou (2000), Murray, Truss & Wynn (2002) and Foulkes, Haswell & Murray (2006) suggest that the negative superhump modulation is related to a warped accretion disc. Patterson et al. (1993) suggest that negative superhumps can be produced by a partially tilted disc. Wood et al. (2000) and Montgomery (2004) and this work show that entire disc tilts can generate negative superhumps in light curves.

A third unknown is how the disc retrogradely precesses. Both Patterson et al. (1993) and Harvey et al. (1995) suggest that retrograde precession in a tilted disc could be from gravitational effects similar to those on the Earth by the Moon and the Sun that cause the Earth to retrogradely precess (Stacey 1977). Harvey et al. (1995) suggest that the secondary exerts a gravitational torque that causes the disc to slowly precess retrogradely but the gravitational torque will cause the tilted disc to re-align with the orbital plane. The idea of a disc's retrogradely precessing line of nodes can be traced to Katz (1973), an idea that is debated in Kondo, Wolff & van Flandern (1983). Bonnet-Bidaud, Motch & Mouchet (1985), continuing the debate, argue for a freely precessing disc and suggest this type of disc for TV Col. This freely precessing disc model is then adopted by Barrett et al. (1988) for TV Col, then by Patterson et al. (1993) for CVs that show photometric signals at the retrograde precession periods and then by, for example, Harvey et al. (1995).

A fourth unknown is which portion of the disc is warped or tilted and thus which portion of the disc is in retrograde precession. Either the tilted edge of a disc freely precesses due to the tidal field of the secondary (Katz 1973) or the secondary precesses due to the tidal field of the primary and the tilted disc retrogradely precesses as a consequence (Roberts 1974). Either the inner disc is tilted, the outer disc is tilted, the entire disc is tilted or the disc is warped. Wood et al. (2000) and Montgomery (2004) show that fully tilted accretion discs precess in the retrograde direction.

A fifth unknown is the source to disc tilt or warp. Accretion discs have been suggested to tilt or warp via a potpourri of sources. In some CVs, a disc tilt can be held constant by a gas stream fed by the magnetic field of the secondary (Barrett et al. 1988). A disc tilt instability can result from a coupling of an eccentric instability to Lindblad resonances (Lubow 1992). A vertical resonant oscillation of the disc midplane can be caused by tidal interactions between a massive secondary and a coplaner primary (Lubow & Pringle 1993). A warping instability can be caused by irradiation from the primary (Pringle 1996, 1997). A warping can be caused by direct tidal forces by a secondary that is orbiting on an inclined orbit. A disc warp can be caused by misalignments of the spin axis of a compact and/or a magnetized primary and the disc axis. In this work, we adopt no particular theory or otherwise make no statement in this work as to how the disc becomes misaligned with the orbital plane, saving this for future work. We do acknowledge that Murray & Armitage (1998) find that CV DN accretion discs do not seem to tilt out of the orbital plane by instabilities.

In addition to the unknowns, observations reveal several differences between positive and negative superhump modulations. Negative superhump modulations in light curves have a period that is slightly shorter than the orbital period, known as the negative superhump period P_-, whereas positive superhumps have a period slightly longer than the orbital period. Unlike positive superhumps, negative superhumps do not seem to be hampered by mass ratio limits as they are found in short orbital period systems like AM CVn (see Fig. 1) and in long orbital period systems like TV Col (see NLs in Fig. 2). Negative superhumps also seem to be prevalent among the SW Sex and VY Scl NL systems (see Fig. 2). A third difference is the shape of the pulse – negative superhumps have a more equilateral triangular shape. A fourth difference is precession – negative superhumps are found in systems that seem to only retrogradely precess and in systems that seem to simultaneously precess both progradely and retrogradely (e.g. TT Ari).

A more complete theory on negative superhumps and retrograde precession needs to address the unknowns as well as the observational differences. In addition, the theory needs to explain how one accretion disc can simultaneously precess both progradely and retrogradely. Because our previous work is so successful in generating negative superhumps and a retrogradely precessing disc, we continue to study fully tilted accretion discs in this work. This work alone does not address all the unknowns and observations, but it does suggest a viable solution.

In this work, we provide a portion of our atlas on simulated negative superhumps and study the source to the negative superhump. For the atlas, we vary mass ratio and maintain disc particle number, particle shape, viscosity, mass transfer rate and primary mass for all simulations. According to Paczynski (1977), a mass ratio $q = M_2/M_1 \leq 0.25$ is necessary if the tidal truncation radius R_{tides} is to lie outside the 3:1 eccentric inner Lindblad resonance radius $R_{3:1}$ for the disc to experience apsidal precession and for the light curve to show positive superhumps. Patterson et al. (2005) find the critical ratio to be more like $q \sim 0.3$ based on observational studies. Montgomery (2001), and references within, shows that positive superhumps can be generated in systems up to a mass ratio of $q = 0.33$, and observational results of BB Doradus (Patterson et al. 2005) tentatively agree. Because we do not wish to study apsidal precession and positive superhumps in this work, we limit this work to a mass ratio range $0.35 \leq q \leq 0.55$. For the atlas, we tilt the disc $5°$. In this work, we also study the source to the negative superhump modulation by varying the degree of disc tilt. In Section 2 of this paper, we introduce the code and input parameters. In Section 3, we suggest a source to the negative superhump modulation. In Section 4, we provide a portion of our atlas on negative superhump numerical simulations, and in Section 5, we compare our numerical simulation results with results obtained from various observed systems. In Section 6, we provide a summary and conclusions.

2 THE SMOOTHED PARTICLE HYDRODYNAMICS CODE

Smoothed particle hydrodynamics (SPH) is a Lagrangian method that models highly dynamical, astrophysical fluid flow as a set of interacting particles (see Monaghan 1992 for a review). In SPH, the local fluid properties at position r, a position also occupied by a particle, are found by sampling nearby fluid elements that are also particles and then weighting their contributions by a smoothing kernel. The Monaghan & Lattanzio (1985) interpolating smoothing kernel W adopted in the Simpson (1995) code mimics a Gaussian but is defined to go to zero beyond a distance of $2h$, where h is the

smoothing length and also the radius of a particle. The code utilizes the simplest SPH form – constant and uniform h and constant and uniform mass particles. In Montgomery (2004), to increase the number of particles in the direction normal to the disc midplane and to increase the number of nearest neighbours to each particle, we modify the particle size and shape from spherical to oblate spheroidal while maintaining the original particle volume. Although the number of particles did increase in the z-direction and better packing in the disc is found, no appreciable improvements in results are seen. Thus, to improve resolution, we increase particle number to 100 000 while maintaining spherical particles of constant radius. To increase computational efficiency, individual particles are advanced through six possible time-steps, the longest of which is $\delta t_1 = P_{orb}/200$ and the shortest of which is $\delta t_6 = 2^{-5}\delta t_1$ as described in Simpson (1995). The choices of time-steps are determined by the particle's local environment. In system units, the orbital period is normalized to $P_{orb} = 2\pi$.

The code models hydrodynamics of an ideal gamma-law equation of state $P = (\gamma - 1)\rho u$, where P is pressure, γ is the adiabatic index, ρ is density and u is specific internal energy. The sound speed is $c_s = \sqrt{\gamma(\gamma - 1)u}$. The momentum and internal energy equations per unit mass are, respectively,

$$\frac{d^2 \mathbf{r}}{dt^2} = -\frac{\nabla P}{\rho} + \mathbf{f}_{visc} - \frac{GM_1}{r_1^3}\mathbf{r}_1 - \frac{GM_2}{r_2^3}\mathbf{r}_2 \tag{1}$$

and

$$\frac{du}{dt} = -\frac{P}{\rho}\nabla \cdot \mathbf{v} + \epsilon_{visc} \tag{2}$$

in their most general form (Simpson 1995). In these equations, t is time, G is the universal gravitational constant, $\mathbf{v}$ is velocity, $\mathbf{f}_{visc}$ is the viscous force, ϵ_{visc} is the energy generation due to viscous dissipation and $\mathbf{r}_1$ and $\mathbf{r}_2$ are the displacements from stellar masses M_1 and M_2, respectively. The momentum and energy equations in SPH form for particles i and j are, respectively,

$$\frac{d^2 \mathbf{r}_i}{dt^2} = -\sum_j m_j \left(\frac{P_i}{\rho_i^2} + \frac{P_j}{\rho_j^2}\right)(1 + \Pi_{ij})\nabla_i W_{ij}$$
$$-\frac{GM_1}{r_{i1}^3}\mathbf{r}_{i1} - \frac{GM_2}{r_{i2}^3}\mathbf{r}_{i2} \tag{3}$$

and

$$\frac{du_i}{dt} = -\mathbf{a}_i \cdot \mathbf{v}_i \tag{4}$$

or if the last equation fails in preventing negative internal energies,

$$\frac{du_i}{dt} = \frac{P_i}{\rho_i^2}\sum_j m_j(1 + \Pi_{ij})\mathbf{v}_{ij} \cdot \nabla_i W_{ij}. \tag{5}$$

In these equations, $\mathbf{a}$ is acceleration, Π_{ij} is the Lattanzio et al. (1986) artificial viscosity:

$$\Pi_{ij} = \begin{cases} -\alpha\mu_{ij} + \beta\mu_{ij}^2 & \mathbf{v}_{ij} \cdot \mathbf{r}_{ij} \leq 0 \\ 0 & \text{otherwise,} \end{cases} \tag{6}$$

where

$$\mu_{ij} = \frac{h\mathbf{v}_{ij} \cdot \mathbf{r}_{ij}}{c_{s,ij}(r_{ij}^2 + \eta^2)} \tag{7}$$

and $c_{s,ij} = \frac{1}{2}(c_{s,i} + c_{s,j})$ is the average sound speed, $\mathbf{v}_{ij} = \mathbf{v}_i - \mathbf{v}_j$, $r_{ij} = r_i - r_j$ and $\eta^2 = 0.01h^2$ as shown in Simpson & Wood (1998).

For our numerical simulations, we choose $\alpha = \beta = 0.5$. Our viscosity is approximately equivalent to a Shakura & Sunyaev (1973) viscosity parametrization ($\nu = \alpha'c_sH$, where H is the disc scale-height) $\alpha' = 0.05$. As Smak (1999) estimates $\alpha' \sim 0.1$–0.2 for DN

systems in high viscosity states, our simulations are more for quiescent systems. As only approaching particles feel the viscous force and since neither radiative transfer nor magnetic fields are included in this code, all energy dissipated by the artificial viscosity is transferred into changing the internal energies. As radiative cooling is not included in this code, the adiabatic index $\gamma = 1.01$ is incorporated to prevent internal energies from becoming too large. By summing the changes in the internal energies of all the particles over a specific time interval n, variations in the bolometric luminosity yield an approximate and artificially generated light curve:

$$L_n = \sum_i du_i^n. \tag{8}$$

In all simulations, an accretion disc is generated by injecting mass from the inner Lagrange point L_1. We inject five particles per major time-step, 200 major time-steps per orbit or a total of 1000 particles per orbit. This mass is accreted on to the primary star through an accretion disc. The gravitational potential is treated as the sum of two-point masses orbiting a common centre of mass that is located at the origin of the coordinate system. In system units, the distance between the centres of the masses is set to an orbital separation $a = 1.0$. All calculations are made in the inertial frame, thus eliminating Coriolis forces. The injection velocity is based on an injection temperature $T_{inj} = 4 \times 10^4$ K and is approximately the sound speed that has been scaled to system units. The code adopts an approximate secondary mass–radius relation $R_2 = (M_2/M_\odot)^{-13/15}$ R$_\odot$ that applies for $0.08 \leq M_2 \leq 1.0$ (Warner 2003). In this relation, R_2 and M_2 are in solar radii and solar mass, respectively.

For our simulations, we assume a primary mass $M_1 = 0.8$ M$_\odot$ and vary the secondary mass M_2 such that $0.35 \leq q \leq 0.55$. For example, if $q = 0.4$ then $M_2 = 0.32$ M$_\odot$ and our simulation unit length-scales to $a \sim 1.23$ R$_\odot$, where we have used the secondary mass–radius relationship found in Warner (2003) and the Eggleton (1983) volume radius of the Roche lobe secondary:

$$\frac{R_2}{a} = \frac{0.49q^{2/3}}{0.6q^{2/3} + \ln(1 + q^{1/3})}. \tag{9}$$

The Eggleton (1983) relation is good for all mass ratios, accurate to better than 1 per cent. Knowing the orbital separation, the orbital period could be found using Newton's version of Kepler's Third Law, but instead we adopt a Smith & Dhillon (1998) secondary mass–period relation:

$$\frac{M_2}{M_\odot} = (0.038 \pm 0.0003)P_{orb}^{1.58 \pm 0.09}, \tag{10}$$

where P_{orb} is in hours. For $q = 0.4$, the orbital period is $P_{orb} \sim 3.85$ h. Taking the radius of the primary to be 6.9×10^8 cm, the scaled radius of the white dwarf is $R_1 = 0.0081a$.

To obtain physical mass accretion rates, we set the particle mass at $m_p = 2 \times 10^{14}$ kg and assume a monatomic hydrogen gas, equal mass particles of equal radius h and equal shape particles. As particles are injected at a rate of 1000 per orbit until 100 000 particles are obtained in the disc, then the mass transfer rate is $\dot{m} \sim 2 \times 10^{-10}$ M$_\odot$ yr^{-1} for our $q = 0.4$ simulation.

A unique feature of this code is the conservation of disc particle number. Any time a particle is accreted on to the secondary or primary mass or is lost from the system, a new particle is injected through L_1. We build a disc of 100 000 particles and maintain this number throughout the simulation as we model systems in steady state. After building the disc, we artificially rotate the disc out of the orbital plane 1°, 2°, 3°, 4°, 5° or 20° at orbit 200 to simulate a tilted disc system. We then allow the disc to evolve in the
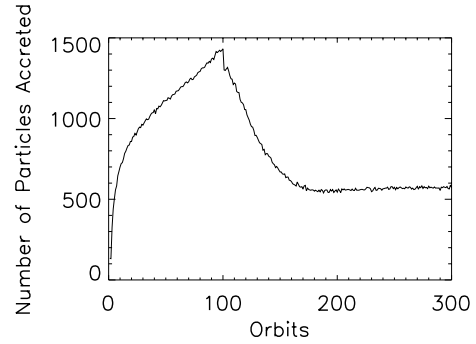

Figure 3. Accretion rate as the disc is building to orbit 100 and as the disc settles into a quasi-equilibrium state beyond orbit 100. The disc maintains 100 000 particles to mimic an SU UMa in quiescence and steady state.

short term to a quasi-equilibrium state where particles are injected at the rate they are removed from the system by either being accreted on to the primary or the secondary or lost from the system. The average net rate of accretion for a quasi-static disc is around 500 per orbit as shown in Fig. 3. As this net rate is approximately half that injected to build the disc, the steady-state mass transfer rate reduces to $\dot{m} \sim 1 \times 10^{-10}$ M$_\odot$ yr^{-1} or a rate similar to an SU UMa in quiescence as shown in Fig. 2. We estimate the density of the gas near L_1 to be $\rho \sim 10^{-10}$ g cm^{-3} using $m_p = (4/3)\pi h^3 \rho$. As we maintain 100 000 particles in the steady-state disc, then the total mass of the disc is $M_{disc} = 100\,000 \times m_p = 3.5 \times 10^{22}$ g or $M_{disc} \sim 2 \times 10^{-11}$ M$_\odot$, a negligible value compared to the mass of either star.

If we assume the outer radius of the disc is $R_{disc} \approx 2\,r_{circ}$, or twice the circularization radius (Warner 2003) where

$$\frac{r_{circ}}{a} = 0.0859q^{-0.426} \tag{11}$$

and $0.05 \leq q < 1$, then for $q = 0.4$, we find $r_{circ} \sim 0.13a$ and $R_{disc} \sim 0.25a$. As $\rho \ll M_{disc}R_{disc}^{-3}$, self-gravity is neglected in these simulations.

To maintain a respectable number of nearest neighbours (≥ 25), we adjust the smoothing length so that it now depends on the mass ratio q. Specifically, h is 1/90 of the distance between the inner Lagrange point L_1 and M_1, i.e. $h = 0.011a$. As explained in Simpson (1995), the code is three-dimensional. Each layer in the z-direction is of uniform thickness $2h$ and the entire simulation is contained within a rectangular prism that is centred at the origin. The prism has sides of length $2a$ and depth $0.48a$. Therefore, the geometrically thin disc is divided into approximately 22 layers.

In Fig. 4, we show for our $q = 0.4$ simulation at orbit 150 the relative density as a function of both distance normal to the midplane z and distance from the primary in units of orbital separation. We also show the height of particles above the midplane and the fractional internal energy production as a function of distance from the primary. In this figure, the disc has 100 000 particles and the mean number of nearest neighbours is 64. We note that at orbit 150, the disc has not yet been tilted. As expected, the maximum density is along the midplane of the disc and peaks near the edge of the disc and the internal energy peaks in the middle of the disc. The average height of the disc above the midplane as a function of distance from the primary roughly follows that of an isothermal axisymmetric disc to a distance $\sim 0.2a$. Beyond this distance, the non-axisymmetric disc and the influence of the secondary breaks the scaling.
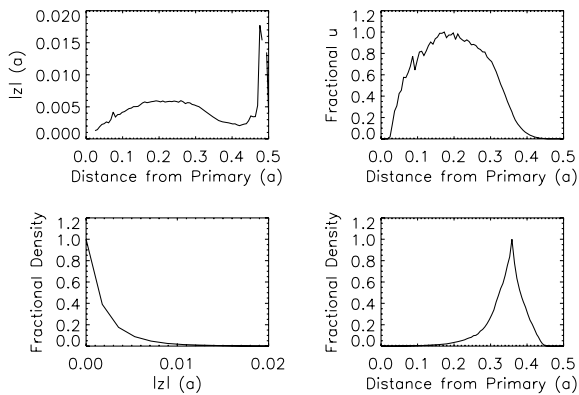
Figure 4. Average height of particles above the midplane as a function of radius (upper left-hand panel), fractional internal energy per mass as a function of radius (upper right-hand panel), fractional density as a function of height z above the midplane (lower left-hand panel) and fractional density as a function of radius (lower right-hand panel) for our $q = 0.4$ simulation at orbit 150. The disc maintains 100 000 particles.

3 SOURCE TO NEGATIVE SUPERHUMP MODULATION

3.1 Catalyst to negative superhumps

In Wood et al. (2000), we show that negative superhumps can be generated in an artificial light curve when the disc is tilted 5° out of the orbital plane. However, we did not establish the minimum disc tilt that would result in statistically significant negative superhump modulations. Once this minimum disc tilt is established, we can further study the role of the gas stream in the generation of negative superhumps.

To find the minimum disc tilt in our $q = 0.4$ simulation, we stop the simulation at orbit 200, artificially rotate the disc by one or more degrees and then restart the simulation. We use a Fourier transform of the last 100 orbits in the light curve as a test of whether or not negative superhumps are significantly present in the disc. The Fourier transform of 100 orbits for 2°, 3° and 4° disc tilts is shown in Fig. 5.

Although a negative superhump signal is present in all three panels, it is not significantly above the noise until the disc is tilted above 3°. In Montgomery (2004), we found for 25 000 particle simulations a similar result. Murray & Armitage (1998) started
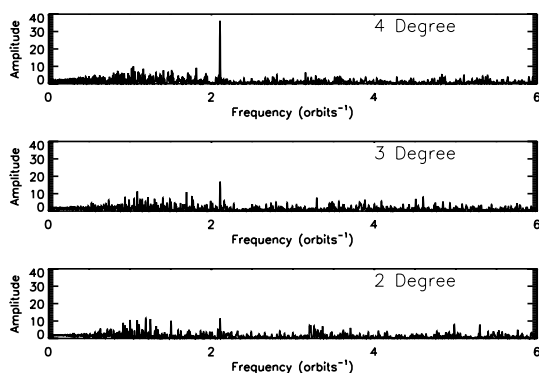

Figure 5. Fourier transform of artificial light curves for $q = 0.4$ simulation where the disc has been tilted 2°, 3° or 4° out of the orbital plane. Simulations are 100 orbits in duration. Units of time are orbits, therefore units of frequency are orbits^{-1}.
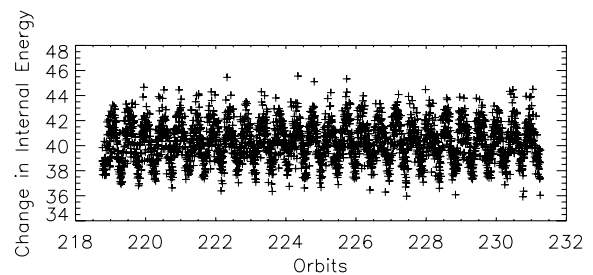

Figure 6. Light curve from an accretion disc that has been tilted 20° out of the orbital plane at orbit 200. In this simulation, $q = 0.4$. Two negative superhump modulations are shown per orbit.

with a 29 592 particle disc and did not find enough strength due to an inclination instability to naturally tilt the disc significantly above 2°, even with an added 1° tilt. Therefore, a few degree tilt as a minimum seems to be in agreement with a negative superhump modulation to be statically present.

Note in the figure that the amplitude of the signal increases with increasing disc tilt and the growth is similar to that of a second-order polynomial. Wood & Burke (2007) found that increasing the mass transfer rate also increases the amplitude and to that we add increasing disc tilt. A higher amplitude signal indicates a more well-defined negative superhump modulation in the light curve. For example, in Fig. 6, we show orbits 220 to 230 of our $q = 0.4$ simulation. In this figure, two well-defined negative superhump modulations are found per orbit with maximums occurring near, for example, orbits 220 and 230 and minimums occurring near, for example, orbit 225. The second maximum or minimum occurs approximately 1/2 orbit earlier or later in each example.

To generate this figure, we tilted the disc 20° at orbit 200 such that the line of nodes is perpendicular to the line connecting the primary and secondary centre of masses, herein referred to as the line of centres. Therefore, the line of centres is parallel to the disc's line of antinodes. As the secondary orbits the centre of mass in the counter clockwise direction, the secondary travels roughly one-quarter of an orbit when it encounters the disc's line of nodes. Travelling nearly another quarter orbit, the line of centres is once again perpendicular to the line of nodes and parallel to the disc's line of antinodes and the secondary encounters a disc face but this time the secondary is facing the other side of the disc. After travelling nearly three quarters of an orbit, the secondary once again meets the disc's line of nodes, and after travelling nearly one full orbit, nearly to orbit 201, the secondary once again encounters the disc's line of antinodes. At this time, the secondary is facing the same side of the disc that the secondary encountered at orbit 200. During this one orbit, the gas stream interacted with the disc edge twice at the bright spot (i.e. at the disc's line of nodes) and twice with the disc face (i.e. at the disc's line of antinodes). The cycle continues as the secondary orbits with the gas stream flowing over the disc for nearly one-half orbit and then transition to flowing under the disc for nearly another one-half orbit.

Because the negative superhump modulation is well defined in this high disc tilt simulation, the varying kinetic energy of the gas stream as it impacts the face of the disc through a locus of points as the secondary orbits (Barrett et al. 1988) may be the source to the negative superhump. To test this idea, we find where the gas stream strikes the disc when the disc is tilted a minimum disc tilt that leads to statistically significant negative superhump modulations (i.e. 4°). In Fig. 7, we show disc side views for our $q = 0.4$ simulation. We
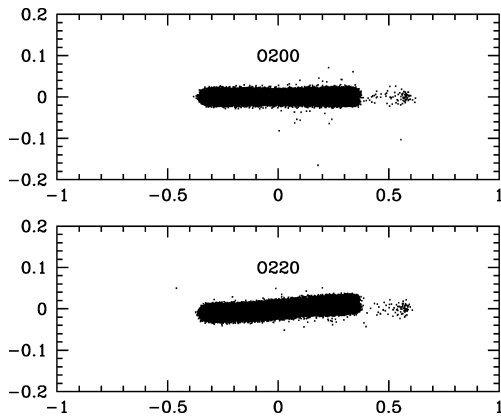
Figure 7. Edge-on views of the gas stream striking the bright spot of a non-tilted disc (upper panel) and a disc that has been tilted $4°$ at orbit 200 (lower panel). The upper panel is the $q = 0.4$ simulation at orbit 200 before the disc is artificially tilted and the lower panel is the simulation at a later time, orbit 220. In both panels, the aspect ratio is exaggerated to emphasize the role of the gas stream in the generation of negative superhumps from a minimally tilted disc.

Figure 8. Folded bolometric light curve of orbits 200–300 for our $q = 0.4$ simulation, where the disc has been tilted $5°$ out of the orbital plane.

compare untilted and tilted discs. In both panels, the secondary is not shown but we show the gas stream leaving the inner Lagrange point and striking the disc. In the top panel, we show orbit 200 (O200) of an untilted disc and thus the accretion stream is striking the disc at the bright spot as expected. Some of the gas particles flow both above and below the disc after striking the disc rim. In the bottom panel, we show orbit 220 (O220) when the disc is emitting its maximum negative superhump modulated light (refer to Fig. 6). As shown, the gas stream is striking the lower half of the disc edge yet still at the bright spot, and more of the gas particles flow under the disc than over the disc. As negative superhumps are statistically significant from a disc tilted $4°$, we conclude that the gas stream does not have to impact the face of the disc in a locus of points to generate negative superhumps. We do acknowledge that negative superhumps cannot be present without the gas stream. In Fig. 7, the aspect ratio is exaggerated to emphasize the role of the gas stream.

As a disc tilt of $4°$ can induce a negative superhump signal well above the noise yet the flared shape of the disc causes the gas stream to mostly strike at the rim of the disc as opposed to cleanly flowing over the disc edge, our results suggest that the bright spot does not necessarily have to transit the face of disc to induce negative superhumps as suggested by others. However, the gas stream that strikes the disc rim and flows mostly over one face of the disc per half orbit does appear to be involved. If the disc is not tilted a few degrees, then the gas stream cannot mostly overflow one face of the disc and negative superhumps are not present. Therefore, as expected, disc tilt of a few degrees is a major catalyst to induce negative superhumps, and without the gas stream, negative superhumps would not be present.

3.2 Location of negative superhump light source

To identify when and where the negative superhump occurs within the disc, we need to find the orbital parameters and the negative superhump phase. From the Fourier transform of orbits 200–300 in our $q = 0.4$ numerical simulation that has been tilted $5°$ about the primary at orbit 200, we identify the negative superhump period to be $P_- = 0.95$ orbits. To convert this period into real units, multiply one orbit by the orbital period $P_{orb} \sim 3.85$ h. Knowing these two

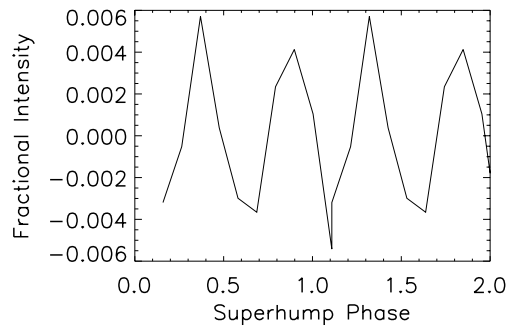periods, we can determine the nodal precessional period by $P_{Pn}^{-1} = P_-^{-1} - P_{orb}^{-1}$ to be $P_{Pn} = 72.2$ h or 19 orbits. Another relation that can be found is the nodal superhump period excess $\epsilon_n = 1 - \frac{P_-}{P_{orb}} = 0.049$. Having identified the negative superhump period to be $P_- = 3.66$ h, we can fold the last 100 orbits on this period to find the negative superhump phase.

In Fig. 8, we show folded superhump light curves from orbits 200–300 for our $q = 0.4$ numerical simulation. Having found two negative superhump modulations per orbit from Fig. 6, we expect to find two negative superhump pulse shapes per orbit in Fig. 8 as our light curves are essentially bolometric, independent of viewing angle or similar to having integrated over 4π sr. Observers typically see only one face of a tilted disc and hence only one superhump modulation per orbit. As shown in this figure, the maximum superhump light occurs approximately before the half-orbit phase ($\phi \sim 0.4$) and full-orbit phase ($\phi \sim 0.9$) and the minimum occurs just before the quarter-orbit and three quarter-orbit phases. Note one pulse amplitude is higher than its half-orbit counterpart.

Knowing the negative superhump maximum phases, we now seek to identify when the disc is emitting this extra light. From Fig. 6, we identified orbits 220 and 230 as examples of approximate maximums and orbit 225 as an example of an approximate minimum for a disc that has been tilted $20°$. As the $q = 0.4$ tilted disc precesses every 19 orbits, other near maximums should occur near orbits 201 and 210 and other near minimums should occur near orbits 206 and 215. With 200 frames per orbit and maximums and minimums occurring nearly every half-orbit as shown in Fig. 6, maximums should occur near frames 0, 100 and 200 of orbits 210, 220 and 230. Likewise, minimums should occur near frames 0, 100 and 200 of orbits 215 and 225. Minimums should also occur near frames 50 and 150 of orbits 210, 220 and 230. Likewise, maximums should also occur near frames 50 and 150 of orbits 215 and 225. As shown in Fig. 7, a maximum occurs when the secondary is nearly in line with the disc's line of antinodes and a minimum occurs when the secondary is nearly in line with the disc's line of nodes, in agreement with theory.

Knowing the approximate orbit and frame when the additional light is being emitted, we now search to identify that portion of the disc that is contributing mostly to the negative superhump modulation. As the disc contributes to most of the light from CV systems, the source to the negative superhump modulation should be from the disc itself, or a portion thereof. As the negative superhump modulation has a higher amplitude and becomes more coherent with increasing disc tilt, we plot in Fig. 9 the sum of each particle's change in internal energy for frame 0 orbit 215 (faint line, lower panel), frame 0 orbit 220 (bold line, lower panel), frame 150 of orbit
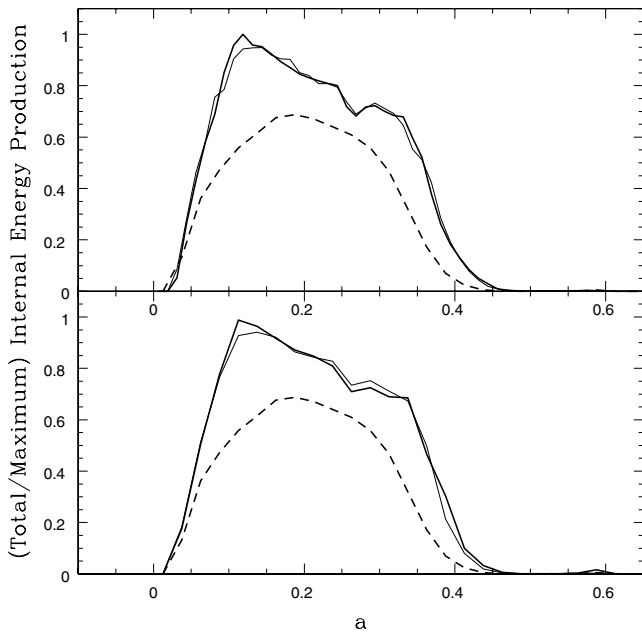
Figure 9. The total change in internal energy is shown as a function of distance from the primary that is located at $a = 0$ for frame 150 of orbit 220 (faint line, upper panel), frame 200 of orbit 220 (bold line, upper panel), frame 0 of orbit 215 (faint line, lower panel) and frame 0 of orbit 220 (bold line, lower panel) of a disc that has been tilted 20°. Frame 0 of orbit 150 for an untilted disc is shown in both panels as dashed lines. The radial distance of each particle from the primary is determined from the Pythagorean theorem.

220 (faint line, upper panel) and frame 200 of orbit 220 (bold line, upper panel) from a disc that has been tilted 20°. The dashed line in both panels is from an untilted disc at frame 0 of orbit 150 like that shown in the upper right-hand panel of Fig. 4.

As shown in Fig. 9, the internal energy distribution from an untilted disc is vastly different than that from a tilted disc. In an untilted disc, the number of particles around $0.1a$ and $0.35a$ is $\sim$600 per bin with each bin of $0.0125a$ equal width. The distribution of the total energy produced resembles a bell curve that is centred near $0.2a$ with $\sim$825 particles contributing to the maximum light. By orbit 215 frame 0, after the disc has been tilted 20° at orbit 200, the number of particles per bin around $0.1a$ and $0.35a$ has increased to $\sim$1200 and $\sim$900, respectively. The distribution of energy production has changed from that of a bell curve to a more linear, negatively sloped curve with more particles emitting more light near $0.1a$. Thus, the inner disc now contributes to most of the light emitted from tilted discs, as expected. A second difference between the untilted and tilted disc fractional light emitted is the notch in the tilted disc curves near $0.27a$. The notch suggests that a ring has formed near $0.27a$ that emits less light than from adjacent annuli, and the source of the cooling ring appears to be from the gas stream striking the disc face.

The largest change between faint and bold lines in the figure occurs near $0.1a$; and thus, this location appears to be the source to the negative superhump modulation. Comparing the curves in Fig. 9, the disc is alternating between nearly minimum states (faint lines – frame 0 of orbit 215 and frame 150 of orbit 220) and nearly maximum states (bold lines – frames 0 and 200 of orbit 220) nearly twice per orbit and this cycle continues through to orbit 300. When the disc is in a maximum state, more light is being emitted near $0.1a$ than when the disc is in a minimum state. With approximately

150 particles per bin and three to four bins, $\sim$500 particles near $\sim0.1a$ are contributing to the additional light when the disc is near a maximum state (bold lines) than when the disc is near a minimum state (faint lines). This number of particles is approximately half the injection rate per orbit for this numerical simulation: approximately 850 particles are lost to the primary and $\sim$100 to the system each orbit, and thus $\sim$950 particles are injected per orbit to maintain 100 000 particles in the disc. Both the number of particles contributing to the negative superhump modulation and the number of particles injected per orbit are few compared to the number of particles within the disc. However, inner annuli are more energetic than outer annuli, and thus more light is emitted per particle from inner annuli. We see from a comparison of frames 0 of orbits 215 and 220 and from frame 150 and frame 200 of orbit 220 that the light emitted from the disc has increased $\sim$5 per cent between $0.1a$ and $0.15a$. If we assume a 5 per cent net increase in disc light, then from $m_1 - m_2 = 2.5 \log \frac{L_2}{L_1}$ we find a 0.053 decrease in apparent magnitude which is within the observed range of 0.03–0.6 mag.

Although we know that the additional negative superhump light occurs near a radius $r = 0.1a$, we have not yet identified whether the emission is from a partial or an entire ring. Therefore, we show in Fig. 10 face-on discs for our $q = 0.4$ simulation. Both panels show orbit 220, frame 80 (additional colour plots in relative density and in relative energy emitted can be found at www.exoplanets.physics.ucf.edu/~montgomery). The panels show energy emitted per particle for a disc tilted 20° (bottom panel, labelled 220.80T) and for an untilted disc (top panel, labelled 220.80). The colour red represents least energetic whereas the colour blue represents more energetic. The gas stream is the colour orange and, therefore, the disc rim is emitting less energy than the gas stream. Note a red cooling ring appears near radius $r \sim 0.27a$, the approximate location where the gas stream strikes the face of the tilted disc. The additional particles emitting more energy from outer annuli, the cooling ring and the additional particles emitting more energy from inner annuli of the tilted disc are in agreement with line curves shown in Fig. 9.

In the untilted disc (top panel, Fig. 10), annuli with radii $r > 0.2a$ alternate colours red and orange whereas annuli with radii $r < 0.2a$ gradually increase in energy released with decreasing radius. In comparison, the tilted disc appears more blended in colour. Annuli with radii $r > 0.2a$ are nearly all at the same energy as that emitted by the gas stream. That is, the alternating red and orange ring pattern found in the outer annuli of the untilted disc is nearly lost in the tilted disc due to the removal of the gas stream striking the disc rim at the bright spot. On the other hand, annuli with radii $r < 0.2a$ in the tilted disc appear more blended because of the increased gas particle migration from outer annuli (e.g. the yellow ring blending with the green ring). In addition, when the disc is tilted 20°, the gas stream strikes the disc face and some of the gas particles skip off the face of the disc towards inner annuli as shown by the additional orange coloured particles in the inner annuli of the tilted disc. Both the additional particle migration and the additional ring of particles that skip off the disc face to inner, more energetic annuli appear to contribute to negative superhump maximum. When the disc is at a negative superhump minimum, the gas stream is striking the bright spot at the disc rim like that shown in the top panel of Fig. 10. Hence, the additional orange coloured particles that skip off the disc face and the additional particle migration to inner annuli that occur when the disc is at a negative superhump maximum are not present.

Our results suggest that as gas particles strike inner, less dense, more energetic annuli, the number of particles increase in that annuli and the disc responds to the increase in number by producing more
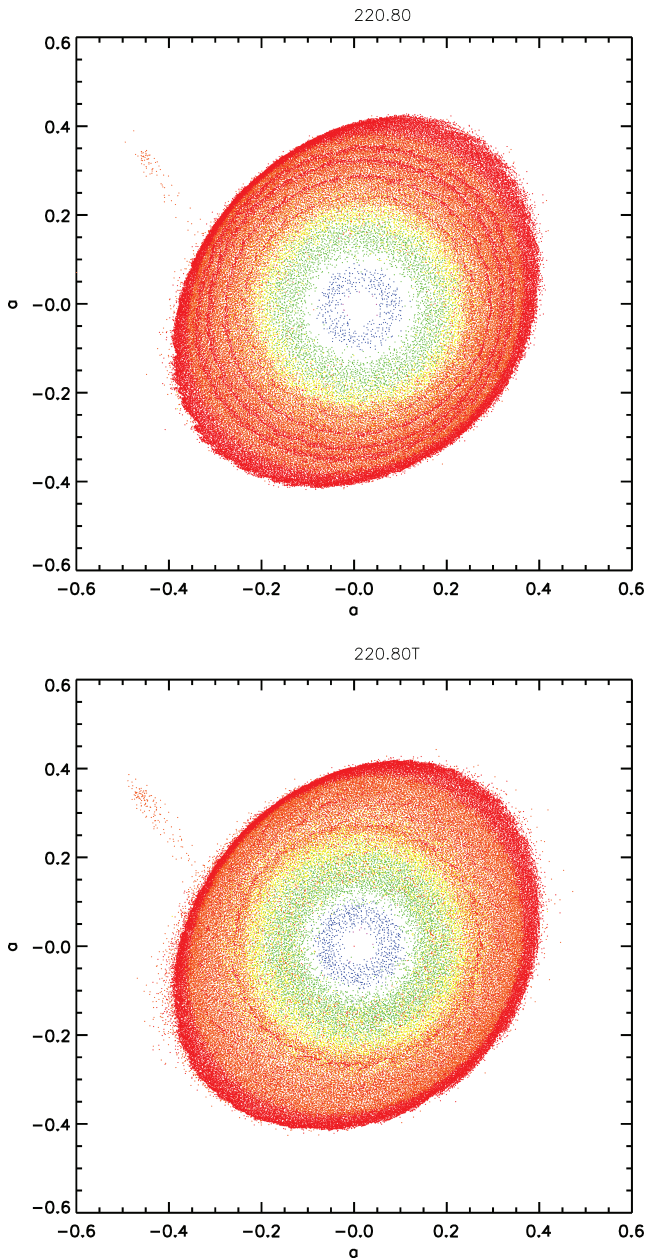
Figure 10. Face-on disc snapshots for $q = 0.4$, orbit 220, frame 80 of a 20° tilted (bottom frame) and an untilted (top frame) disc. The gas stream is the colour orange. The colour red represents less energetic particles whereas blue represents more energetic. Relative internal energies are orange/red ~ 0.6 per cent, yellow/red ~ 4 per cent, green/red ~ 8 per cent, white/red ~ 18 per cent, blue/red ~ 29 per cent and violet/red ~ 83 per cent.

light. The combination of additional particles in inner annuli and the additional light that each particle emits via disc tilt is suggested by our work to be the source of the negative superhump modulation. Wood & Burke (2007) show this inner annuli brightening over one-half orbit although they attribute the additional light to the transit of the bright spot across the face of the disc. Kunze, Speith & Hessman (2001) find inner annuli brightening from their studies of various rates of mass transfer overflowing disc rims, also supporting these results.

3.3 Disc configuration for negative superhumps

Having shown that the disc has to be tilted for the gas stream to overflow a disc face and having identified that the gas particles need to reach the inner, more energetic annuli for the negative superhump modulation to occur, we seek to establish a viable disc configuration that can answer the previously identified unknowns and observations. Others have suggested that the outer disc is tilted, the inner disc is tilted or the disc is warped. We suggest a fully tilted disc.

If the disc is fully tilted about the line of nodes, then the gas stream can overflow one disc face and reach inner, more energetic annuli. As the secondary orbits, each face of the disc can release this additional light nearly once per orbit. Observers would see only one negative superhump modulation if the optically thick disc is more face-on to the observer. A full disc tilt also agrees with the findings that the amplitude of the negative superhump increases with increasing disc tilt or mass transfer rate. If the disc is tilted higher, then the more gas particles can reach inner annuli. If instead the disc tilt is low and the mass transfer rate is high, then more particles can plow through to inner annuli.

A full disc tilt configuration can explain the observed negative superhump periods and nodal percessional periods. It can explain the disc's retrograde precession of the line of nodes, that is the location within the disc where the gas stream transitions from flowing over to flowing under the disc and vice versa. This configuration explains the location within the disc that powers the negative superhump modulation. As this location is different than that which powers the positive superhump modulation, this configuration can explain how both modulations can occur simultaneously within the same disc. Although this work does not address all of the unknowns and observations discussed in the Introduction, it does provide a viable disc configuration that addresses many in the list. A full disc tilt configuration looks promising.

4 NUMERICAL SIMULATION RESULTS

We present in this work a portion of our atlas that focuses on negative superhumps only and thus we present simulations for mass ratios $0.35 \le q \le 0.55$. Fig. 11 shows simulated light curves for these various negative superhump numerical simulations. In all panels of this figure, the disc is created up through orbit 100. After the disc has settled in the short term, the disc is artificially tilted 5° at orbit 200. In all simulations, we see a small rise in internal energy production at orbit 200. This rise is due to the disc tilt. The most significant result is the lack of features from orbits 200 to 300 in all simulations. With a mass transfer rate like that of an SU UMa or a U Gem (see Fig. 2) and with a 5° tilt, the negative superhump modulation is hard to see.

Fig. 12 shows the Fourier transforms to the light curves in Fig. 11. In this figure, the negative superhump signal is found at a frequency greater than two because two superhump modulations are created in our simulations, one per half-orbit, because the secondary encounters the first line of nodes at a negative superhump period that is less than one-half the orbital period and because we effectively integrate over 4π sr to determine the light emitted over time. No harmonics of statistical significance are generated at the mass transfer rate used in these simulations. In simulations with 25 000 particles, (Montgomery 2004) injected at a rate of 2000 particles per orbit, twice that of these simulations, harmonics are generated. Therefore, mass transfer rate is identified to be a source to changing mode frequencies. Also shown in this figure is an increasing amplitude with
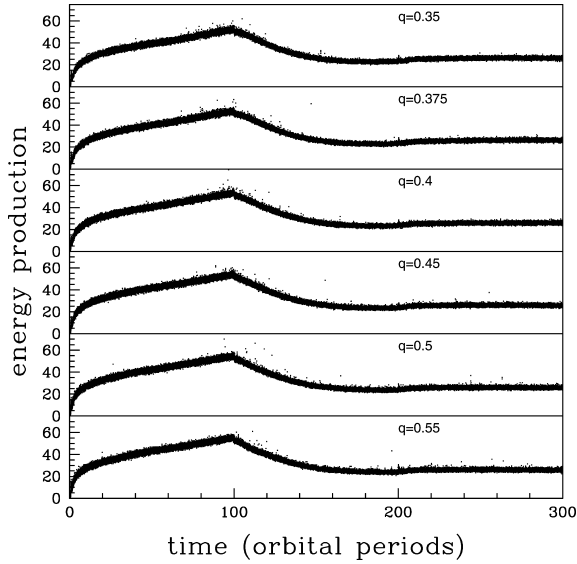
Figure 11. Light curves from accretion discs that have been tilted 5° out of the orbital plane at orbit 200. Mass ratios are shown. Units of orbital periods are orbits.
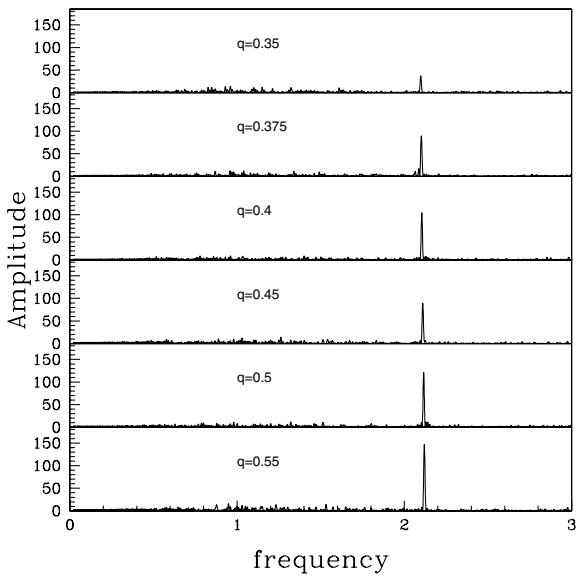

Figure 12. Fourier transforms of light curves in Fig. 11. Mass ratios are shown. Units are orbit^{-1}.

Table 1. Negative superhump simulation data.

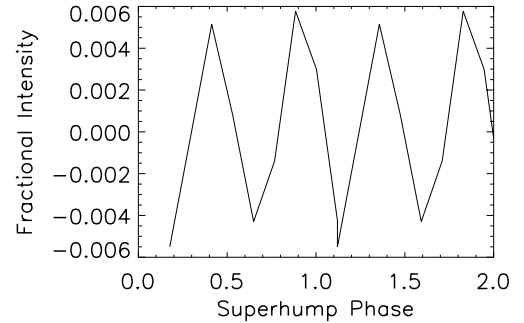| q	Frequency (P_{orb}^{-1})		Period (h)			
	$2\nu_-$	$\sigma_{2\nu_-}$	P_{orb}	P_-	σ_{P_-}	ϵ_n
0.35	2.098	0.004	3.540	3.374	0.006	0.0467
0.375	2.105	0.004	3.698	3.514	0.006	0.0498
0.4	2.104	0.004	3.852	3.662	0.006	0.0494
0.45	2.110	0.004	4.150	3.934	0.007	0.0521
0.5	2.115	0.003	4.436	4.195	0.007	0.0544
0.55	2.119	0.003	4.712	4.447	0.007	0.0562

Figure 13. Folded bolometric light curve of orbits 200–300 for $q = 0.55$ simulation, where the disc has been tilted 5° out of the orbital plane at orbit 200. The unit of the superhump phase is orbits.

representative sample because of the strong signal in the Fourier transform and because of the uniform pulse shapes. To create the pulse shape, the $q = 0.55$ light curve in Fig. 11 is folded on the corresponding negative superhump period given in Table 1 for orbits 200–300. Comparing Figs 8 and 13, we find that negative superhump pulse shapes look similar regardless of mass ratio. We also find that a higher mass ratio results in more similar amplitudes of the $\phi = 0.4$ and 0.9 phases. These results suggest that the light emitted from each face of the disc twice per orbit becomes more equal with increasing mass ratio and thus smaller disc size.

Also of interest is the shape of the pulses as they resemble equilateral triangles like those found from observations. The shape suggests that the modulated light uniformly increases to a maximum and then uniformly decreases to a minimum. As inner annuli supply the extra light, this result suggests that particles within the inner annuli wax and wane their internal energies uniformly as well. As the gas stream that overflows the disc feeds the inner annuli and because we keep the gas stream mass transfer rate fairly constant in our simulations, our results suggest that the equilateral-shaped negative superhumps obtained from observations may involve a time-independent gas stream mass transfer rate.

5 COMPARISONS WITH OBSERVATIONAL DATA AND DISCUSSION

Table 2 lists observational data including orbital periods, negative superhump periods and nodal period excesses for several CV systems. If errors are known, they are listed in parentheses. We select long orbital period systems so that we may compare their observational results with our higher mass ratio numerical simulation results. In the table, NL is nova like, PS is permanent superhumper and IP is intermediate polar.

mass ratio, the strongest of which is from a disc with the smallest radius. Therefore, we can identify mass ratio as a source to increasing the amplitude of the negative superhump modulation in addition to disc tilt and mass transfer rate.

A non-linear least squares fit to each Fourier transform is computed and the standard deviation to twice the negative superhump frequency $2\nu_-$ is found. These data are listed in Table 1 along with the calculated negative superhump period, its propagated error and the nodal superhump period excess. The units for period are hours whereas the units for frequency are orbits^{-1} to be consistent with the Fourier transform figure. To convert to real units, multiply one orbit by the orbital period.

Fig. 13 shows the negative superhump phases for two orbits of our $q = 0.55$ simulation. We show the $q = 0.55$ pulse shape as a

Table 2. Negative superhump observational data and calculated precessional periods and Nodal superhump period excesses.

System	Type	q	P_{orb} (d)	P_{p_n} (d)	P_n (d)	ϵ_n
TV Col[a,b]	IP	0.4 ± 0.05[c]	0.2292	3.973	0.2167	0.0545
V751 Cyg[d]	NL, VY Scul		0.1445 (2)	3.806	0.1394 (1)	0.0353 (2)
PX And[e,f]	NL, SW Sex	0.329 (11)[f]	0.14635 (1)	4.228	0.1415	0.0331
BH Lyn[f,g]	NL, SW Sex	$0.45 + 0.15 - 0.10$[h]	0.15575 (1)	3.413	0.1490	0.0433
		0.301 (15)[f]				
		0.41 ± 0.26[g]				
KR Aur[i]	NL, VY Scul	0.60[j]	0.1628	4.489	0.1571 (2)	0.0350 (2)
AT Cnc[k]	Z Cam, PS	$0.32 - 1.04$	0.2011 (6)	5.051	0.1934 (8)	0.0179 (10)
				11.03	0.1975 (8)	0.0383 (10)
TX Col[l]	IP		0.2375	1.669	0.2083	0.1229
SDSS J040714.78−064425.1[m]	SU UMa?		0.170 17 (3)	6.727	0.166 (1)	0.024 (1)
HS 1813+6122[n]	NL, SW Sex		0.1479	3.166	0.1413	0.0446
V2574 Oph[o]	Nova		0.147 73	3.429	0.14164	0.0412
RX 1643+34[p]	NL, SW Sex		0.120560 (14)	3.917	0.116 96 (8)	0.030 00 (8)

Notes: ?, tentavely assigned candidacy type.
[a]Hellier & Buckley (1993). [b]Retter et al. (2003). [c]Cropper et al. (1999). [d]Patterson et al. (2001).[e]Patterson (1998). [f]Patterson et al. (2005). [g]Dhillon et al. (1992). [h]Hoard & Szkody (1997). [i]Kozhevnikov (2007). [j]Kato, Ishioka & Uemura (2002). [k]Kozhevnikov (2004). [l]Retter, Liu & Bos (2005). [m]Ak et al. (2005). [n]Rodriguez-Gil et al. (2007). [o]Kang et al. (2006). [p]Patterson et al. (2002).
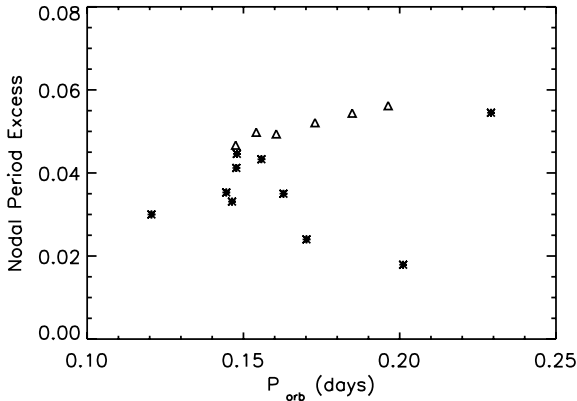

Figure 14. Nodal superhump period excess as a function of orbital period. Observational data are shown as stars and numerical data are shown as triangles. Data are from Tables 1 and 2.

From a quick scan of Table 2, the nodal period excess for TX Col does not follow the trend set by the other observational data. TX Col's orbital period is the longest of the set, longer than TV Col's, and its negative superhump period is not as long. Thus, further observations of this object are suggested and we do not consider this object any more in this study. The tentatively assigned candidacy type of SU UMa for the Sloan object does not agree with its observational period (see Fig. 2) and an observational revisit to this object may also be needed but we do consider this object in our study.

Of the mass ratios that are known, all are higher and nearly all have high-mass transfer rates as implied by their subclasses (see Fig. 2). Excluding the Sloan object, the observational data suggest that negative superhumps are more common in high-mass transfer systems than in low-mass transfer systems. Also, negative superhumps do not seem to be a feature of the U Gem class indicating that U Gem's may be immune to disc tilt.

Fig. 14 shows a comparison of the observational nodal period excess (*) to the numerical nodal period excess (△) values listed in Tables 1 and 2, respectively. The values are compared relative to their orbital periods and errors for orbital periods can be taken as the maximum width of each symbol. Of the observations, HS 1813+6122 agrees reasonably well with our numerical simulation.

Since we simulated a red dwarf secondary using the Smith & Dhillon (1998) secondary mass–period relation, this system may have a red dwarf secondary as it is within the period gap. As the observational data do not suggest a trend, a secondary mass–period relation other than the Smith & Dhillon (1998) utilized in this work may need to be studied for these long orbital period systems.

6 SUMMARY, CONCLUSIONS AND FUTURE WORK

We artificially tilt SPH numerical simulated accretion discs out of the orbital plane by various degrees and for various mass ratios, and we establish their negative superhump periods, orbital periods, nodal precessional periods and nodal superhump period excesses. We confirm our earlier work that tilted discs do wobble and lead to a retrograde precession of the line of nodes. In addition to increased mass transfer rates, we find that increasing disc tilt and higher mass ratios result in higher amplitude and more coherent negative superhump modulations. Simulations of higher mass ratios also show more similar amplitude pulses.

We find that discs need to be tilted a few degrees for the negative superhump to be statistically well above the noise. Discs that are tilted at least a few degrees allow the gas stream to overflow the disc rim and reach inner, less dense, more energetic annuli. These inner annuli wax and wane in emission as the secondary orbits. Thus, the innermost annuli are identified to be the location that powers the negative superhump modulation, a location that is different from that which powers the positive superhump. We find that the minimum disc tilt that results in negative superhump modulations of statistical importance is $4°$. However, because the gas stream still strikes the disc rim at this low disc tilt, our results suggest that the bright spot does not necessarily have to transit the face of the disc for negative superhump modulations to be generated. If the disc tilt is high, however, then the gas stream strikes the disc face and causes a dense, cooling ring to be generated within the disc. The total light emitted as a function of radius has a notch near the location of the gas stream disc interface.

We find that an accretion disc that is entirely tilted around the line of nodes can be a viable disc configuration for systems that show

only negative superhump modulations or both negative and positive superhump modulations. This disc configuration can explain the retrograde precession of the disc's line of nodes, that is the location of where the gas stream transitions from mostly flowing over the disc to mostly flowing under the disc and vice versa. It can also explain how a gas stream can reach inner annuli that power the negative superhump. It can also explain how two modulations can co-exist in the same disc as the modulations occur in different locations within the disc. The apsidal superhump light comes from spiral density waves that extend radially through the disc and we suggest that the negative superhump light comes from inner disc annuli. Future work involves numerical simulations showing how both modulations can occur simultaneously in the same disc. This work also does not explain how accretion discs become tilted, and we save this for future work.

The approximately equilateral triangular shape of the superhump pulse suggests that this additional brightening waxes and wanes uniformly with the constant increase or decrease in gas particles that reach inner annuli of the disc. That is, the uniform shape of the pulse suggests that the mass transfer rate is time-independent. Our results also show that lower mass transfer rates do not generate harmonics.

Negative superhumps are found in observational systems with high-mass ratios, high orbital periods and high-mass transfer rates. The U Gem class of CVs seems to be immune to tilted discs. This work does not study SU UMas, and thus we cannot say much further on this class in this study. As no trend is found in negative superhump period excess of observational systems that have long orbital periods, additional secondary mass–period relations other than those studied in this work are suggested.

ACKNOWLEDGMENTS

REFERENCES

Ak T., Retter A., Liu A., Esenoglu H. H., 2005, New Astron., 11, 147
Barrett P., O'Donoghue D., Warner B., 1988, MNRAS, 233, 759
Bonnet-Bidaud J. M., Motch C., Mouchet M., 1985, A&A, 143, 313
Cropper M., Wu K., Ramsay G., Kocabiyik A., 1999, MNRAS, 306, 684
Dhillon V. S., Jones D. H. P., Marsh T. R., Smith R. C., 1992, MNRAS, 258, 225
Eggleton P. P., 1983, ApJ, 268, 368
Foulkes S. B., Haswell C. A., Murray J. R., Rolfe D. J., 2004, MNRAS, 349, 1179
Foulkes S. B., Haswell C. A., Murray J. R., 2006, MNRAS, 366, 1399
Harvey D., Skillman D. R., Patterson J., Ringwald F. A., 1995, PASP, 107, 551
Hellier C., 2001, PASP, 113, 469
Hellier C., Buckley D. A. H., 1993, MNRAS, 265, 766
Hirose M., Osaki Y., 1990, PASJ, 42, 135
Hoard D. W., Szkody P., 1997, ApJ, 481, 433
Kaygorodov P. V., Bisikalo D. V., Kuznetsov O. A., Boyarchuk A. A., 2006, A&A, 419, 1035
Kang T. W., Retter A., Liu A., Richards M., 2006, AJ, 131, 1687
Kato T., Ishioka R., Uemura M., 2002, PASJ, 54, 1033
Katz J. I., 1973, Nature Phys. Sci., 246, 87
Kondo Y., Wolff C. L., van Flandern T. C., 1983, ApJ, 273, 716
Kozhevnikov V. P., 2004, MNRAS, 290, 490
Kozhevnikov V. P., 2007, MNRAS, 378, 955
Kunze S., Speith R., Hessman F., 2001, MNRAS, 322, 499
Lasota J.-P., 2001, New Astron. Rev., 45, 449
Lattanzio J. C., Monaghan J. J., Pongracic H., Schwarz M. P., 1986, J. Sci. Stat. Comput., 7, 591
Lubow S. H., 1991a, ApJ, 381, 259
Lubow S. H., 1991b, ApJ, 381, 268
Lubow S. H., 1992, ApJ, 398, 525
Lubow S. H., Pringle J. E., 1993, ApJ, 409, 360
Meyer F., Meyer-Hofmeister E., 1981, A&A, 104, L10
Monaghan J. J., 1992, ARA&A, 30, 543
Monaghan J. J., Lattanzio J. C., 1985, A&A, 149, 135
Montgomery M. M., 2001, MNRAS, 325, 761
Montgomery M. M., 2004, PhD thesis, Florida Institute of Technology
Murray J. R., 1996, MNRAS, 279, 402
Murray J. R., Armitage P. J., 1998, MNRAS, 300, 561
Murray J. R., Truss M. R., Wynn G. A., 2002, in Gänsicke B. T., Beuermann K., Reinsch K., eds, ASP Conf. Ser. Vol. 261, Modelling Unstable Accretion Discs. Astron. Soc. Pac., San Francisco, p. 416
Osaki Y., 1985, A&A, 144, 369
Osaki Y., 1989, PASJ, 41, 1005
Paczynski B., 1977, ApJ, 216, 822
Patterson J., 1998, PASP, 110, 1132
Patterson J., 1999, in Mineshige S., Wheeler J. C., eds, Disk Instabilities in Close Binary Systems. Universal Academy Press, Tokyo, p. 61
Patterson J., Thomas G., Skillman D., Diaz M., 1993, ApJS, 86, 235
Patterson J., Kemp J., Saad J., Skillman D. R., Harvey D., Fried R., Thorstensen J. R., Ashley R., 1997, PASP, 109, 468
Patterson J., Thorstensen J. R., Fried R., Skillman D. R., Cook L. M., Jensen L., 2001, PASP, 113, 72
Patterson J. et al., 2002, PASP, 114, 1364
Patterson J. et al., 2005, PASP, 117, 1204
Petterson J., 1977, ApJ, 216, 827
Pringle J. E., 1996, MNRAS, 281, 357
Pringle J. E., 1997, MNRAS, 292, 136
Retter A., Hellier C., Augusteijn T., Naylor T., Bedding T. R., Bembrick C., McCormick J., Velthuis F., 2003, MNRAS, 340, 679
Retter A., Liu A., Bos M., 2005, ASSL, 332, 251
Roberts W. J., 1974, ApJ, 187, 575
Rodriguez-Gil P. et al., 2007, MNRAS, 377, 1747
Shakura N. I., Sunyaev R. A., 1973, A&A, 24, 337
Simpson J. C., 1995, ApJ, 448, 822
Simpson J. C., Wood M. A., 1998, ApJ, 506, 360
Smak J., 1999, Acta Astron., 49, 391
Smith R. C., 2006, Contemp. Phys., 47, 6
Smith D. A., Dhillon V. S., 1998, MNRAS, 301, 767
Smith A. J., Haswell C. A., Murray J. R., Truss M. R., Foulkes S. B., 2007, MNRAS, 378, 785
Stacey F. D., 1977, Physics of the Earth, 2nd edn. John Wiley & Sons, New York
Terquem C., Papaloizou J. C. B., 2000, A&A, 360, 1031
Vogt N., 1982, ApJ, 252, 653
Warner B., 2003, Cataclysmic Variable Stars. Cambridge Univ. Press, Cambridge
Whitehurst R., 1988a, MNRAS, 232, 35
Whitehurst R., 1988b, MNRAS, 233, 529
Whitehurst R., 1994, MNRAS, 266, 35
Whitehurst R., King A. R., 1991, MNRAS, 249, 25
Wood M. A., Burke C. J., 2007, ApJ, 661, 1042
Wood M. A., Montgomery M. M., Simpson J. C., 2000, ApJ, 535, L39

This paper has been typeset from a TeX/LaTeX file prepared by the author.